RSC Advances

ROYAL SOCIETY OF CHEMISTRY

www.rsc.org/advances

Cotton-based hollow carbon fibers with high specific surface area prepared by ammonia etching for supercapacitor application

Shuguang Wang, Zhonghua Ren, Jianpeng Li, Yaqi Ren, Lei Zhao and JieYu*

Shenzhen Engineering Lab of Flexible Transparent Conductive Films, Shenzhen Key Laboratory for Advanced Materials, and Department of Material Science and Engineering, Shenzhen Graduate School, Harbin Institute of Technology, University Town, Shenzhen 518055, China.

**Corresponding author. E-mail: jyu@hitsz.edu.cn*

Fax: +86-755-26033504

Tel: +86-755-26033478

Abstract

In this paper, carbon fibers with a high specific surface area (SSA) have been prepared from cotton for supercapacitor application. The cotton-based carbon fibers (CCFs) are prepared by carbonizing the cotton fibers in ammonia (NH_3) and nitrogen gases at different temperatures. The CCFs possess hollow tubular structure with outer diameter at about 7 μm and inner diameter at about 3 μm. The hollow structure is inherited from the natural structure of the cotton fibers. The SSA and pore structure of the CCFs depend on the carbonizing temperature and atmosphere. The CCFs carbonized in NH_3 have high SSA up to 778.6 m^2 g^{-1} with higher mesopore ratio. Higher nitrogen concentration (3.3 at.%) and more C=O functional groups are present in the CCFs carbonized in NH_3. The maximum specific capacitance of the CCFs carbonized in NH_3 are measured to be 355 F g^{-1} at 1 A g^{-1}, 245.3 F g^{-1} at 0.8 A g^{-1}, and 181.3 F g^{-1} at 0.2 A g^{-1} in KOH, H_2SO_4, and Na_2SO_4 electrolytes, respectively. The tubular structure, high SSA, higher mesopore ratio, nitrogen doping, and the presence of the oxygen functional groups are responsible for the excellent electrochemical performance. Comparing with the conventional activation process using KOH as an etchant the present process by NH_3 etching to prepare the high SSA carbon materials has the advantages of simplicity,

no contaminants, and higher mesopore ratio.

Keywords: cotton fibers; carbon fibers; supercapacitors; specific capacitance; specific surface area

1. Introduction

Supercapacitors with the advantages of high power capability, long cycle life, and fast charge/discharge rate are now attracting ever increasing interest due to their applications in many areas such as portable electronics, electric vehicles, and pulsing techniques.[1-4] According to the charge storage mechanism, supercapacitors can be classified into electrical double layer capacitors (EDLCs) and pseudocapacitors. The former store charges by reversible ion adsorption on the electrode surface and the later do by fast reversible Faradic reactions between the electrode materials and the electrolyte.[5-8] The main requirement for the electrode materials of the EDLCs is high effective surface area because of the charge storage mechanism based on the ion accumulation on the electrode surface. Carbon materials such as activated carbon,[9, 10] carbon nanotubes,[10, 11] carbon nanofibers,[12, 13] graphene[14], and carbide-derived carbon[15] are generally used to fabricate the EDLCs for their high specific surface area (SSA). Among the different carbon materials activated carbon has been widely used in commercial production of supercapacitors due to its low cost and high SSA. Conventionally, the activated carbon is prepared from coal and those dense plant materials such as wood and nut shells. However, the specific capacitance and energy density of the conventional activated carbon is not high because of its microporosity and random pore structure.[16-19] As a matter of fact, there exists a rich variety of plant materials with various microstructures, which may provide good precursors for preparing carbon materials suitable for supercapacitor application. Recently, different plant materials such as rice husk,[20] leaves,[21] banana fibers,[22] tea-leaves,[23] and seaweeds[24] have been used as the precursors to prepare the carbon materials for pursuing superior structure and property for supercapacitor application. For example, the carbon materials obtained by simple

pyrolysis of the seaweeds possesses a SSA of 1307 m^2 g^{-1} and specific capacitance of 175 F g^{-1} in 1 M H_2SO_4 solution even without using activation process.[24] Comparing with other synthetic routes preparation of novel carbon structure from the natural structure of plant materials is inexpensive, simple, high-yielding, and environment-friendly. However, the research on preparation of carbon materials from plant resources is not enough now and further work is necessary to find better plant resources and improve the preparing process.

Cotton is an ordinary plant material with attractive fiber morphology, which can serve as the precursor to prepare the CFs. In contrast, the common plant resources as listed above can only produce the carbon materials with granular morphology. The conventional CFs are generally prepared from pitch or polyacrylonitrile, which have been used for supercapacitor application after activation and shows better electrochemical performance than the granular activated carbon due to the fibrous morphology.[25, 26] The conventional CFs have also been widely used as substrates for growing different active materials due to their excellent conductivity and flexibility.[27] Comparing with the conventional CFs the cotton-based CFs (CCFs) is hollow and may have better electrochemical performance when used as the active materials due to the increased surface area. Anyway, the CCFs derived from cotton provide alternative selection for supercapacitor application due to the green nature and low cost. Recently, highly flexible supercapacitors have been fabricated using the CCFs prepared from cotton fibers, but the specific capacitance is only 12–14 F g^{-1} because of the low SSA.[28] At present, the preparation of the CCFs with high SSA and excellent supercapacitor performance have not been well investigated and thus further work is necessary to exploit the capability of the CCFs by modifying their structure.

In this paper, the CCFs with hollow structure, high SSA, and doped nitrogen (N) have been prepared from cotton by one-step carbonization in ammonia (NH_3) gases. The high SSA of the CCFs is caused by the etching reaction of NH_3 with carbon at high temperature. The CCFs exhibit excellent electrochemical performance including high

specific capacitance, high energy density, and high operation stability for supercapacitor application in different electrolytes, which can be ascribed to the high SSA, high mesopore ratio, and N doping generated by the NH_3 etching as well as the hollow structure. Comparing with the conventional production procedures of the activated carbon including carbonization in protection atmosphere and activation with chemical reagents such as KOH the preparation of the CCFs with high SSA by NH_3 etching can be accomplished in one step. To the best of our knowledge, this is the first time to prepare the N doped CCFs with high SSA by NH_3 etching. The present CCFs deserve attention considering the abundance of cotton.

2. Experimental

The cotton was obtained from Hualu Company in Shandong province. The applied electrolytes of KOH, H_2SO_4, and Na_2SO_4 are analytical grade. The carbonization of the cotton fibers was carried out in a conventional tube furnace. During carbonization the cotton fibers were heated for 2 h at 700, 800, and 900 ^oC with a heating rate of 5 ^oC min^{-1} in NH_3 atmosphere with a flow rate of 100 mL min^{-1}. For comparison, the cotton fibers were also carbonized in N_2 atmosphere following the above described procedure.

The prepared CCFs were characterized by scanning electron microscope (SEM, HITACHI S-4700), X-ray diffractometer (XRD, Rigaku D/Max 2500/PC), Raman spectroscopy (Renishaw RM-1000), and transmission electron microscope (TEM, JEM-2100HR). The SSA and pore structure were determined by nitrogen adsorption at 77 K (Micromeritics TriStar 3020). The total SSA and micropore SSA were calculated using the BET method and t-plot method, respectively. The pore size distribution curves were calculated using the Barrett−Joyner−Halenda (BJH) method. X-ray photoelectron spectroscopy (XPS, ESCALAB 250) was used to determine the composition. The electrical conductivity of the CCFs was mesurred by a multimeter using a conventional setup for measuring powder materials (Fig. 1).[21] The thermogravimetric (TG) curve was measured by a TG analyzer (STA449F3, Jupiter).

The electrochemical performance of CCFs was evaluated on an electrochemical workstation (CHI760C, Shanghai Chenhua Instrument Co. Ltd, China) in a three-electrode system in different aqueous electrolytes (6 M KOH, 1 M H_2SO_4, and 1 M Na_2SO_4 solutions). For the measurements in alkaline and neutral electrolytes, the working electrodes were prepared by directly pressing the CCFs (about 4 mg cm^{-2}) onto nickel foam. For preparing the electrodes for the measurements in acidic electrolyte, the CCFs (about 2 mg cm^{-2}) were coated on glassy carbon substrate by dripping a drop of nafion solution (5 wt.% in water, Alfa Aesar). During measurements a platinum plate and an Hg/HgO electrode were used as the counter and reference electrode, respectively. Cyclic voltammetry (CV) curves, galvanostatic charge/discharge (CD) curves, and electrochemical impedance spectra (EIS) were measured to evaluate the supercapacitive performance.

The specific capacitance and energy density were calculated by the following formulas:[2, 12]

$$C_{SP} = I \times \Delta t / (\Delta V \times m)$$

$$E = 1/2 \times C_{SP} \times (\Delta V)^2 / 3.6$$

where C_{sp} (F g^{-1}) is the specific capacitance of the active materials, I (A) is the discharge current, ΔV (V) is the potential window of discharge, Δt (s) is the discharge time, m (g) is the mass of the active material, E (Wh kg^{-1}) refers to the energy density of the active materials.

3. Results and discussion

In order understand the thermal property of cotton TG analysis was performed. Fig. 2 shows the TG curve of cotton measured in N_2 from room temperature to 900 ^oC. It can be seen that the weight decreases rapidly from 300 ^oC and keeps stable after 400 ^oC. The final carbon yield is about 29%. The optical image of the applied cotton is shown in Fig. 3a. After carbonization the obtained CCFs shrink, but show about similar shape to the original cotton without obvious break (Fig. 3b). Fig. 3c and d show the typical SEM

images of the CCFs. The fiber morphology of the cotton is well preserved for the CCFs. The average diameter of the CCFs is about 7 μm, about similar to the Nomex aramid CFs.[26] From the cross section of a fractured fiber it is observed that the CCFs is hollow, presenting a microtubular structure (Fig. 3d). The inner diameter and the wall thickness of the CCF tube are about 3 μm and 1.5 μm, respectively. The hollow structure of the CCFs is superior to the solid structure of the conventional CFs when used as the supercapacitor electrodes because the inner surface may contribute to the charge storage.

Fig. 4a shows the XRD patterns of the CCFs carbonized at different temperatures in different atmosphere. All the patterns exhibit the characteristic of turbostratic carbon with the two peaks at about 24.6 ^{o} and 43.8^{o}, corresponding to the diffraction of (002) and (100) planes. For the samples carbonized in NH_3 the (002) peak narrows with increasing the carbonizing temperature (patterns II-IV), indicating improvement of crystallinity at higher temperature. Comparing with the samples carbonized in NH_3 the sample carbonized in N_2 at 800 ^{o}C shows a broader peak width, suggesting that NH_3 could promote the crystallization of the CCFs.[12, 30, 31] Fig. 4b shows the corresponding Raman spectra of the CCFs carbonized at different temperatures in different atmosphere. Two broad peaks can be observed around 1345 and 1591 cm^{-1}, corresponding to the well-known D and G peaks of carbon associated with the disordered and graphitized structure, respectively. The spectra indicate the characteristics of microcrystalline graphitic materials.[31] The integrated intensity ratio of D to G peak (I_D/I_G) was obtained by Lorentzian fitting, which can be used to estimate the crystallinity of the carbon materials. The I_D/I_G ratios of the CCFs carbonized in NH_3 at 700, 800, and 900 ^{o}C are 2.09, 1.83, and 1.56, respectively, confirming the crystallinity improvement at higher temperature. The I_D/I_G ratio of the CCFs carbonized in N_2 at 800 ^{o}C is 2.02, confirming the promoting effect of NH_3 and high temperature on the crystallization of the carbon materials. The present Raman results are in agreement with those indicated by the above XRD.

Fig. 5a is the low magnification TEM image showing the typical morphology of the CCFs. Although the tube wall is very thick for the electron transmission the tubular structure of the CCFs can still be observed. The inner and outer diameters of the CCF shown in Fig. 5a are 3 and 7 μm, respectively, which is about similar to the observation by SEM images. Fig. 5b and c show the high resolution TEM (HRTEM) images of the CCFs carbonized at 800 ^{o}C in NH_3 and N_2, respectively. It is observed that both samples are highly defective although some desultory and distorted lattice fringes corresponding to the graphitic (002) plane can be seen.

Table 1. Calculated total SSA (S_t, m^2 g^{-1}), micropore SSA (S_m, m^2 g^{-1}), total pore volume (V_t, cm^3 g^{-1}), micropore volume (V_m, cm^3 g^{-1}), average pore size (d_a, nm), and percentage of the micropore SSA (P_m) for the CCFs prepared at different temperatures in different atmospheres.

Temperature (^{o}C)	Atmosphere	S_t	S_m	V_t	V_m	d_a	P_m
700	NH_3	318.2	292.7	0.163	0.145	5.21	92.0%
800	NH_3	602.1	491.4	0.369	0.243	4.43	81.6%
900	NH_3	778.6	594.3	0.410	0.292	3.45	76.3%
800	N_2	108.3	108.2	0.065	0.056	28.79	99.9%

The N_2 adsorption/desorption isotherms of the different samples are shown in Fig. 6a. It is indicated that for the CCFs carbonized in NH_3 the adsorption capacity increases greatly with increasing the carbonizing temperature, reflecting the increase of the SSA. The abrupt rise of the isotherm at very low P/P_0 value is caused by the adsorption of the micropores while the subsequent gradual increase with increasing the relative pressure originates from adsorption of the mesopores. It is observed that the isotherm of the CCFs carbonized at 800 ^{o}C in NH_3 exhibits an apparent adsorption/desorption hysteresis loop above the P/P_0 value of 0.45, which are caused by the capillary condensation in mesopores and macropores.[32, 33] The calculated results of the pore structure are listed in Table 1. The SSA of the CCFs carbonized at 700, 800, and 900 ^{o}C in NH_3 are 318.2, 602.1, and 778.6 m^2 g^{-1}, respectively. In contrast, the CCFs carbonized in N_2 at 800 ^{o}C

possess much lower adsorption capacity with a SSA of 108.3 $m^2 g^{-1}$, suggesting that the high SSA of the CCFs carbonized in NH_3 is due to the presence of NH_3. At high temperature NH_3 can decompose into H containing active species such as atomic H and NH_x ($x \leq 2$), which react with carbon to produce volatile products, resulting in the porous structure and high SSA. The large tails appearing in all the isotherms in the high relative pressure range near 1.0 is related to indicating the presence of the mesopores and macropores.[31, 32] It is noted that the CCFs etched by NH_3 possess higher mesopore and macropore percentage than the activated carbon prepared by the KOH etching,[33] which is beneficial to the supercapacitor application.[16] Pore size distribution of the CCFs is shown in Fig. 6b. As indicated in Table 1, for the CCFs carbonized in NH_3 the micropore percentage decreases with increasing the carbonizing temperature, namely, the total percentage of the mesopores and macropores increases. This tendency has also been observed for the preparation of the activated carbon by KOH activation, where micropore volume decreases as the carbonizing temperature of the precursors increases.[34] However, from Fig. 4b it is found that the percentage of the mesopores above 3 nm and macropores is higher for the CCFs carbonized at 800 ^oC than those carbonized at 900 ^oC. The pore distribution of the 800 ^oC CCFs shows a strong peak from 3 to 4.5 nm. It is considered that the higher percentage of the mesopores above 3 nm and the macropores accounts for the adsorption/desorption hysteresis loop for the CCFs carbonized at 800 ^oC in NH_3.

The electrical conductivity of the active materials is an important parameter for supercapacitor application. The conductivity of CCFs carbonized at 700, 800, and 900 ^oC in NH_3 and 800 ^oC in N_2 were determined to be 0.0070, 0.014, 0.039, and 0.0075 S cm^{-1}, respectively (Fig. 1). It is found that the conductivity increases with increasing the carbonizing temperature for the CCFs carbonized in NH_3 and the CCFs prepared in NH_3 have higher conductivity than those prepared in N_2 at similar temperature. XPS spectra were measured to investigate the composition and surface functional groups of the CCFs as they play important roles in the electrochemical process of charge storage. Fig.

7 shows the XPS spectra of the CCFs carbonized at 800 ^{o}C in NH_3 and N_2. It is found that both the samples contain C, N, and O elements. The concentrations (at%) of C, O, and N are 88.18%, 8.52%, and 3.30% for the CCFs carbonized in NH_3 and 89.28%, 10.50%, and 0.32% for the CCFs carbonized in N_2, respectively. By deconvoluting the O1s spectra it is found that the O element may exist in the forms of C=O, C-O-C, C-O-H, COOH, and H_2O (Fig. 7b).[12, 35, 36] According to the literatures the C=O group will contribute to the electrochemical capacitance by introducing Faradic reaction.[35, 36] As indicated in Fig. 7b, the content of the C=O group is higher in the CCFs carbonized in NH_3 than those carbonized in N_2. Furthermore, both samples are doped with N and the CCFs carbonized in NH_3 have higher N content (Fig. 7c).

Electrochemical performance of the CCFs was first evaluated in 6 M KOH solution with a three-electrode system. Fig. 8a shows the CV curves of the different samples. The CV curves exhibit nearly rectangular shape, indicating the charge storage characteristics of the EDL. For the CCFs carbonized in NH_3 the current response first increases and then decreases with increasing the carbonizing temperature with the maximum occurring at 800 ^{o}C. Comparing with the CCFs carbonized in NH_3 at 800 ^{o}C the CCFs carbonized in N_2 at 800 ^{o}C exhibit much lower current density. Fig. 8b shows the CD curves of the different samples. All the CD curves display the capacitive characteristic for charge storage with nearly triangular shape.[12] By calculation from the CD curves the specific capacitance of the CCFs carbonized in NH_3 at 700, 800, 900 ^{o}C and in N_2 at 800 ^{o}C are 142.6, 355.0, 204.2, and 133.2 F g^{-1} at the current density of 1 A g^{-1}, respectively, and the energy densities are 28.5, 71.0, 40.8, and, 26.6 Wh Kg^{-1}, respectively. The above changing trend is related to the SSA and pore structure of the CCFs. Generally, higher SSA results in the higher specific capacitance for the EDLCs. However, it is noted that despite the lower SSA for the CCFs carbonized in NH_3 at 800 ^{o}C than those at 900 ^{o}C the former possess much higher specific capacitance than the later. This confirms that pore size plays key roles in the charge storage of the EDLCs.[16, 34, 37] The higher specific capacitance obtained for the CCFs carbonized in NH_3 at 800 ^{o}C

may originate from the higher proportion of mesopores with size above 3 nm mainly, suggesting that the mesopores above 3 nm may be more effective for ion transport. This result should be valuable for the design and preparation of the electrode materials of supercapacitors. Fig. 8c and d are the CV curves measured at different scan rates and the CD curves measured at different current densities of the CCFs carbonized at 800 ^{o}C in NH_3. The nearly rectangular shape was kept with slight distortion with increasing the scan rate for the CV curves and the CD curves exhibit nearly triangular shape at all current densities, indicating the efficient capacitive behavior and good charge propagation across the electrodes.[14, 37-39] The specific capacitance calculated from the CV curves of the CCFs carbonized at 800 ^{o}C in NH_3 is 323.3, 300.2, 267.5, and 213.4 F g^{-1} at the scan rates of 5, 10, 20, and 50 mV s^{1}, respectively, and the values calculated from the CD curves are 355.0, 340.1, 310.5, and 254.4 F g^{-1} at the current densities of 1, 2, 4, and 8 A g^{-1}, respectively.

The EIS spectra of the different samples and an equivalent circuit are shown in Fig. 10, which were measured in the frequency range of 0.01-100 kHz with an AC perturbation of 5 mV. All the Nyquist plots show similar shape with a rough semicircle in the high frequency region, a straight line in the low frequency region, and a Warburg section (W) of 45^{o} slope in the middle frequency region. The semicircle results from the parallel connection of charge transfer resistance (R_{CT}) at the electrode/electrolyte interface and double-layer capacitance. The intercept of the semicircle with the real axis at high frequency side corresponds to the internal resistance (Rs) including the resistances of the electrolyte solution, electrode material, and the electrode material/current collector interface, among which the main part is from the electrolyte solution.[20] The internal resistances are about 2.22, 1.49, 1.12, and 2.67 Ω for the CCFs carbonized in NH_3 at 700, 800, and 900 ^{o}C and in N_2 at 800 ^{o}C, respectively. For the CCFs carbonized in NH_3 the internal resistance is comparable to other carbon materials.[12, 20, 40] It is expected that the internal resistance could be reduced by adding conductive additives. The decrease of the internal resistance with increasing carbonizing

temperature is mainly caused by the improvement of crystallinity at higher temperature.[18] The semicircle diameter reflects the magnitude of R_{CT}, which decreases with increasing the carbonizing temperature. This should be caused by the increased contact area between the electrode structure and the electrolyte solution due to the higher SSA at higher temperature. The low frequency straight line is related to the ion diffusion resistance in the electrode materials, which should exhibit a vertical shape for an ideal capacitor.[15, 28] Similar to the changing trend of the specific capacitance, the low frequency straight line of the CCFs carbonized in NH_3 at 800 ^oC has the largest slope. This should be also a consequence of the higher proportion of the mesopores above 3 nm, which are more efficient for ion transport.[20, 41] In addition to the KOH electrolyte the electrochemical performance in 1 M H_2SO_4 and 1 M Na_2SO_4 solutions were also evaluated on the CCFs carbonized at 800 ^oC in NH_3, which are shown in Fig. 9. Both CV curves in the two electrolytes exhibit nearly rectangular shape, indicating the charge storage characteristics of the EDL. The maximum specific capacitance and energy density were calculated from the CD curves of the samples, which are 245.3 F g^{-1} and 27.6 Wh kg^{-1} at 0.8 A g^{-1} in H_2SO_4 solution and 181.3 F g^{-1} and 56.7 Wh kg^{-1} at 0.2 A g^{-1} in Na_2SO_4 solution.

Cyclic stability is of great importance for the practical application of supercapacitors. Fig. 11 shows the specific capacitance vs. cycle number curves of the CCFs carbonized in NH_3 at 800 ^oC in 6 M KOH, 1 M H_2SO_4, and 1 M Na_2SO_4 electrolytes, which were measured at the current densities of 4 A g^{-1}, 2 A g^{-1}, and 2 A g^{-1}, respectively. It is indicated that the CCFs have high operation stability in alkaline, acidic, and neutral electrolytes. The capacitance retention of the CCFs after 4000 cycles reaches 92.4%, 102.5%, and 94.1% in KOH, H_2SO_4, and Na_2SO_4 solutions, respectively. The present work manifests that the CCFs prepared from cotton possess excellent electrochemical performance including high specific capacitance, high energy density, and high operation stability in alkaline, acidic, and neutral electrolytes. The excellent electrochemical performance can be mainly ascribed to the higher mesopore ratio and

the hollow structure of the CCFs. The presence of the surface oxygen groups and the N doping contribute also to the excellent electrochemical performance.[12, 35, 36, 42] Comparing with the route to prepare the activated carbon with KOH activation the present one-step process by NH_3 etching is simpler and impurity-free.

Conclusions

In summary, the CCFs with tubular structure, high SSA, and high N content has been prepared from cotton by carbonization. The tubular structure of the CCFs is inherited from the natural structure of cotton fibers. The SSA and pore structure of the CCFs are strongly dependant on the carbonizing temperature and atmosphere. High SSA up to 778.6 m^2 g^{-1} has been obtained by carbonization in NH_3, which is ascribed to the etching reactivity of NH_3 with carbon. Comparing with the activation process with KOH the present one-step process by NH_3 etching is simpler and impurity-free and can generate higher mesopore ratio, and dope N. The CCFs possess excellent electrochemical performance including high specific capacitance, high energy density, and long-term stability in alkaline, acidic, and neutral electrolyte. The mesopores above 3 nm was found to contribute greatly to the excellent electrochemical performance. On account of the abundance of the cotton materials (including the waste cotton cloth) the present CCFs are expected to play roles in the application of supercapacitors.

Acknowledgments

This work is supported by the National Basic Research Program of China (2012CB933003), National Natural Science Foundation of China (No. 51272057), and Shenzhen Basic Research Program (JCYJ20130329150737027).

Reference

1 E. Frackowiak, Phys. *Chem. Chem. Phys.*, 2007, **9**, 1774-1785.

2 P. Simon and Y. Gogotsi, *Nat. Mater.*, 2008, **7**, 845-854.

3 L. L. Zhang and X. S. Zhao, *Chem. Soc. Rev.*, 2009, **38**, 2520-2531.

4 G. P. Wang, L. Zhang and J. J. Zhang, *Chem. Soc. Rev.*, 2012, **41**,797-828.

5 Y. Gogotsi and P. Simon, *Science*, 2011, **334**, 917-918.

6 N. Padmanathan and S. Selladura, *RSC Adv.*, 2014, **4**, 8341–8349.

7 E. Frackowiak and F. Beguin, *carbon*, 2001, **39**, 937-950.

8 L. Zhao, J. Yu, W. J. Li, S. G. Wang, C. L. Dai, J. W. Wu, X. D. Bai and C. Y. Zhi, *Nano Energy*, 2014, **4**,39-48.

9 F. X. Wang, S. Y. Xiao, Y. Y. Hou, C. L. Hu, L. L. Liu and Y. P. Wu, *RSC Adv.*, 2013, **3**, 13059-13084.

10 V.V.N. Obreja Vasile, *Physica E: Low-dimensional Systems and Nanostructures*, 2008, **40**, 2596-2605.

11 Q. Zhang, J. P. Rong, and B. Q. Wei, *RSC Adv*., 2011, **1**, 989–994

12 L. Zhao, Y. J. Qiu, J. Yu, X. Y. Deng, C. L. Dai and X. D. Bai, *Nanoscale*, 2013, **5**, 4902-4909.

13 C. Tran and V. Kal a, *J. Power Sources*, 2013, **235**, 289-296.

14 Y. W. Zhu, S. Murali, M. D. Stoller, K. J. Ganesh, W. W. Cai, P. J. Ferreira, A. Pirkle, R. M. Wallace, K. A. Cychosz, M. Thommes, D. Su, E. A. Stach and R.S. Ruoff, *Science*, 2011, **332**, 1537-1541.

15 C. R. Pérez, S. H. Yeon, J. Ségalini, V. Presser, P. L. Taberna, P. Simon and Y. Gogotsi, *Adv. Funct. Mater.*, 2013, **23**, 1081-1089.

16 J. Huang, B. Sumpter and V. Meunier, *Chem. Eur. J.*, 2008, **14**, 6614-6626.

17 C. Ma, Y. Song, J. Shi, D. Zhang, X. Zhai, M. Zhong, Q. Guo and L. Liu, *Carbon*, 2013, **51**, 290-300.

18 J. Gamby, P. L. Taberna, P. Simon, J. F. Fauvareque and M.Chesneau, *J. Power Sources*, 2001, **101**, 109-116.

19 Z. Chen, D. Weng, H. Sohn, M. Cai and Y. F. Lu, *RSC Adv.*, 2012, **2**, 1755-1758.

20 X. J. He, P. H. Ling, M. X. Yu, X. T. Wang, X. Y. Hang and M. D. Zheng, *Electrochim. Acta*, 2013, **105**, 635-641.

21 M. Biswal, A. Banerjee, M. Deo and S. Ogale. *Energy Environ. Sci*., 2013, **6**, 1249-1259.

22 V. Subramanian, C. Luo, A. M. Stephan, K. S. Nahm, S. Thomas and B. Q. Wei, *J. Phys. Chem. C*, 2007, **111**, 7527-7531.

23 C. Peng, X. B. Yan, R. T. Wang, J. W. Lang, Y. J. Ou and Q. J. Xue, *Electrochim. Acta*, 2013, **87**, 401-408.

24 E. Raymundo-Pinero, M. Cadek and F. Beguin, *Adv. Fun. Mater.*, 2009, **19**, 1032-1039.

25 A. G. Pandolfo and A. F. Hollenkamp, *J. Power Sources*, 2006, **157**, 11-27.

26 K. Leitner, A. Lerf, M. Winter, J. O. Besenhard, S. Villar-Rodil, F. Suarez-Garcia, A. Martinez-Alonso and J. M. D. Tascon, *J. Power Sources,* 2006, **153**, 419-423.

27 N. Padmanathan and S. Selladurai, *RSC Adv.*, 2014, **4**, 8341-8349.

28 J. L. Xue, Y. Zhao, H. H. Cheng, C. G. Hu, Y. Hu, Y. N. Meng, H. B. Shao, Z. P. Zhang and L. T. Qu, *Phys. Chem. Chem. Phys.*, 2013, **15**, 8042-8045.

29 X. Q. Wang, J. S. Lee, Q. Zhu, J. Liu, Y. Wang and S. Dai, *Chem. Mater.*, 2010, **22**, 2178-2180.

29 Y. J. Qiu, J. Yu, T. N. Shi, X. S. Zhou, X. D. Bai and J. Y. Huang, *J. Power Sources*, 2011, **196**, 9862-9867.

30 Y. J. Qiu, J. Yin, H. W. Hou, J. Yu and X. B. Zuo, *Electrochim. Acta*, 2013, **96**, 225-229.

31 F. Tuinstra and J. L. Koenig, *J. Chem. Phys.*, 1970, **53**, 1126-1130.

32 S. Alvarez, J. Esquena, C. Solans and A. B. Fuertes, *Adv. Eng. Mater*., 2004, 6, 897-899.

33 Y. J. Qiu, J. Yu, G. Fang, H. Shi, X. S. Zhou and X.D. Bai, *J. Phys. Chem. C*, 2009, **113**, 61-68.

34 E. Raymundo-Pinero, K. Kierzek, J. Machnikowski and F. Beguin, *Carbon*, 2006, **44**, 2498-2507.

35 C. T. Hsieh and H. Teng, *Carbon*, 2002, **40**, 667-674.

36 L. Z. Fan, S. Y. Qiao, W. L. Song, M. Wu, X. B. He and X. H. Qu, *Elctrochim. Acta,* 2013, **105**, 299-304.

37 D. Y. Qu and H. Shi, *J. Power Sources*, 1998, **74**, 99-107.

38 J. J. Yoo, K. Balakrishnan, J. S. Huang, V. Meunier, B. G. Sumpter, A. Srivastava, M. Conway,A. L. M. Reddy, J. Yu, R. Vajtai and P. M. Ajayan, *Nano Lett.*, 2011, **11**, 1423-1427.

39 S. H. Li, L. Qi, L .H. Lu and H. Y. Wang, *RSC Adv.*, 2012, **2**, 3298–3308

40 L. L. Zhang, X. Zhao, M. D. Stoller, Y. Zhu, H. Ji, S. Murali , Y. Zhu, H. J. Ji, S. Murali, Y. P. Wu, S. Perales, B. Clevenger and R. S. Ruoff, *Nano Lett.*, 2012, **12**, 1806-1812.

41 X. J. He, Y. J. Geng, J. S. Qiu, M. D. Zheng, X. Y. Zhang and H. F. Shui, *Energy & Fuels*, 2010, **24**, 3603-3609.

42 L. F. Chen, X. D. Zhang, H. W. Liang, M. G.Kong, Q. F. Guan, P. Chen, Z. Y. Wu and S. H. Yu, *ACS Nano*, 2012, **6**, 7092-7102.

Figure captions

Fig. 1 Conductivity of CCFs synthesized at 700, 800 and 1000 ^{o}C in NH_3 and 800 ^{o}C in N_2 and the inset is the schematic diagram of conductivity measurements under pressure.

Fig. 2 Thermogravimetric curve of cotton fibers.

Fig. 3 Photographs of the applied cotton precursor (a) and the obtained CCFs (b) and SEM images of the CCFs carbonized at 800 ^{o}C in NH_3 atmosphere (c and d).

Fig. 4 XRD patterns (a) and Raman spectra (b) of the CCFs carbonized in N_2 at 800°C (I) and in NH_3 at 700 (II), 800 (III), and 900 °C (IV).

Fig. 5 (a) Low magnification TEM image showing the tubular structure of the CCFs. (b) HRTEM image of the CCFs carbonized at 800 ^{o}C in NH_3. (c) HRTEM image of the CCFs carbonized at 800 ^{o}C in N_2.

Fig. 6 Nitrogen adsorption/desorption isotherms (a) and pore size distribution (b) of the CCFs carbonized at different temperatures in different atmospheres.

Fig. 7 XPS survey spectra (a), O1s spectra (b), and N1s spectra (c) of the CCFs carbonized at 800 ^{o}C in NH_3 and N_2.

Fig. 8 (a) CV curves of the different samples at 20 mV s^{-1}. (b) CD curves of the different samples at 1 A g^{-1}. (c) CV curves of the CCFs carbonized at 800 ^{o}C in NH_3 at different scan rates. (d) CD curves of the CCFs carbonized at 800 ^{o}C in NH_3 at different current densities.

Fig. 9 CV curves of the CCFs carbonized at 800 ^{o}C in NH_3 measured in 1 M H_2SO_4 (a) and 1 M Na_2SO_4 (b) solutions at 20 mV s^{-1}.

Fig. 10 Nyquist plots of the CCFs carbonized at different temperatures in different atmospheres. The inset shows the equivalent circuit.

Fig. 11 Operation stability of the CCFs carbonized in NH_3 at 800^{o}C in different electrolytes.

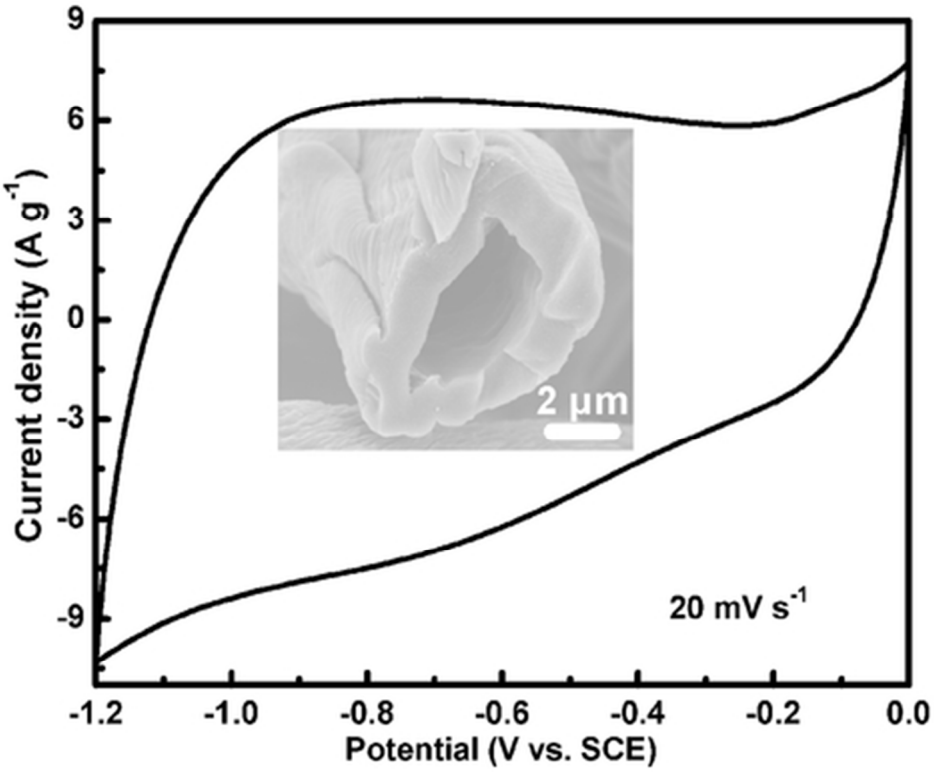

Graphical abstract
39x32mm (300 x 300 DPI)

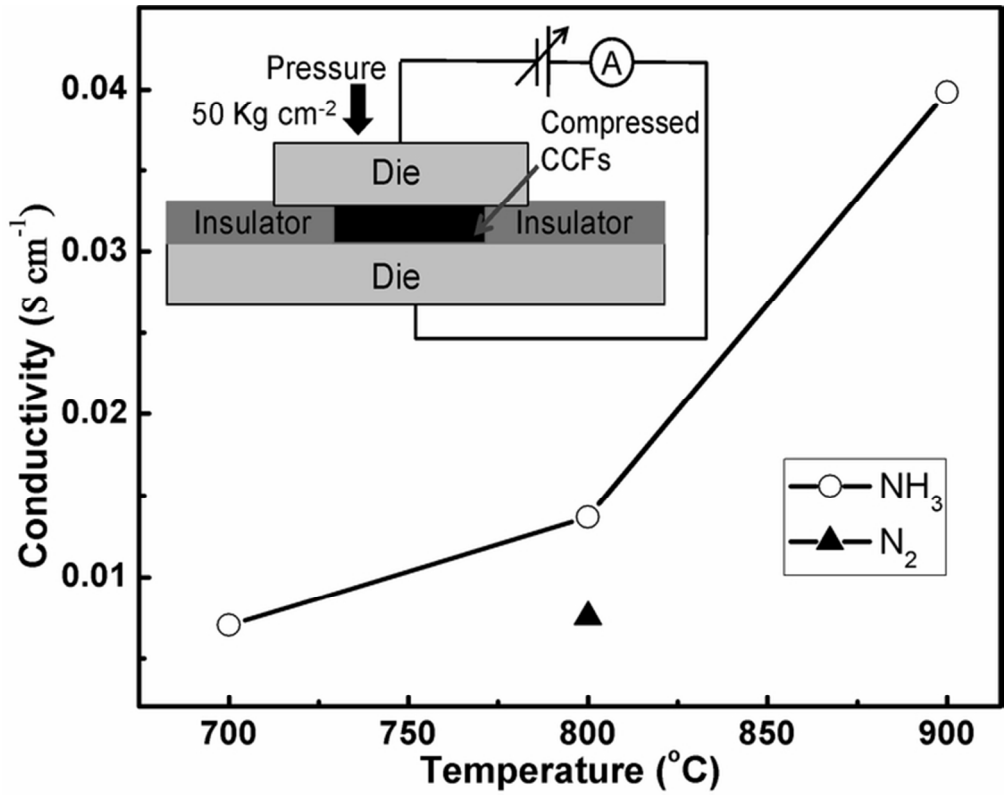

63x49mm (300 x 300 DPI)

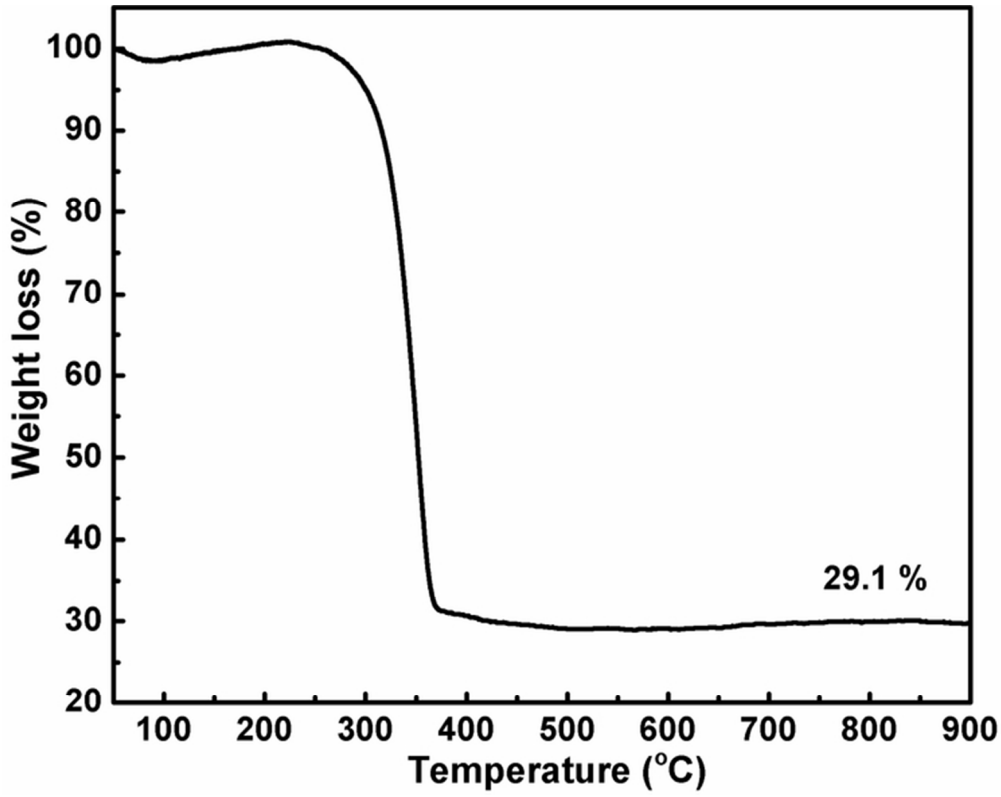

63x49mm (300 x 300 DPI)

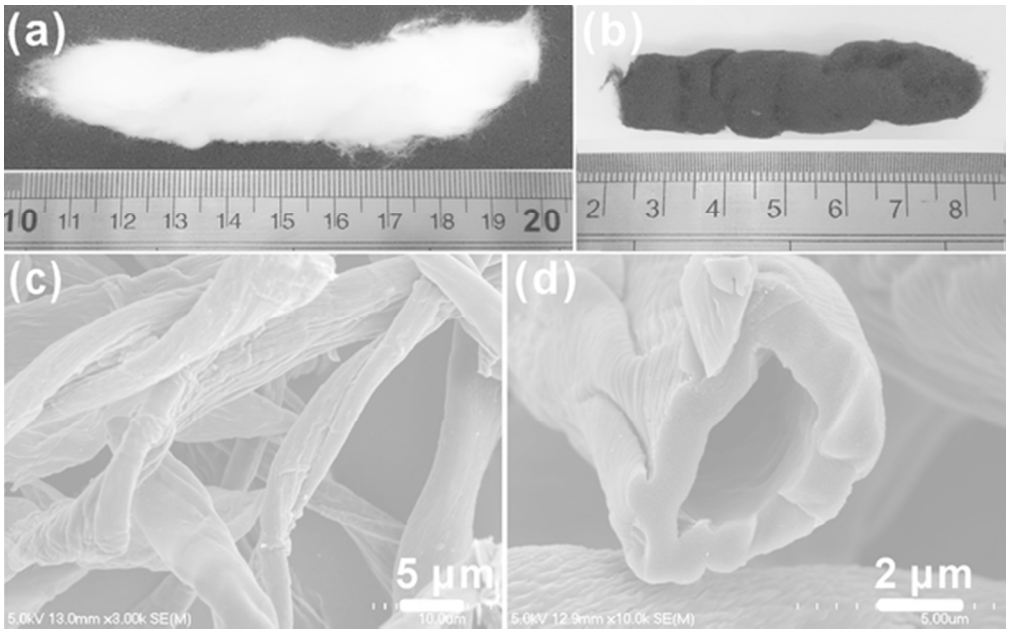

51x32mm (300 x 300 DPI)

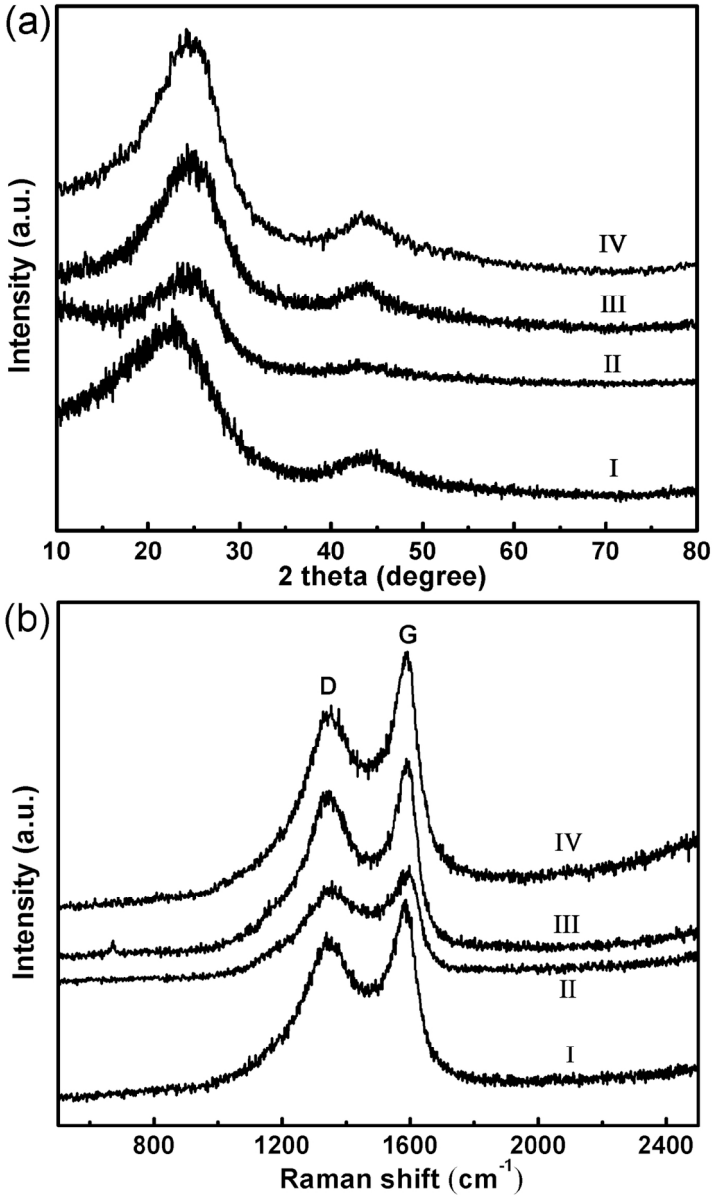

117x197mm (300 x 300 DPI)

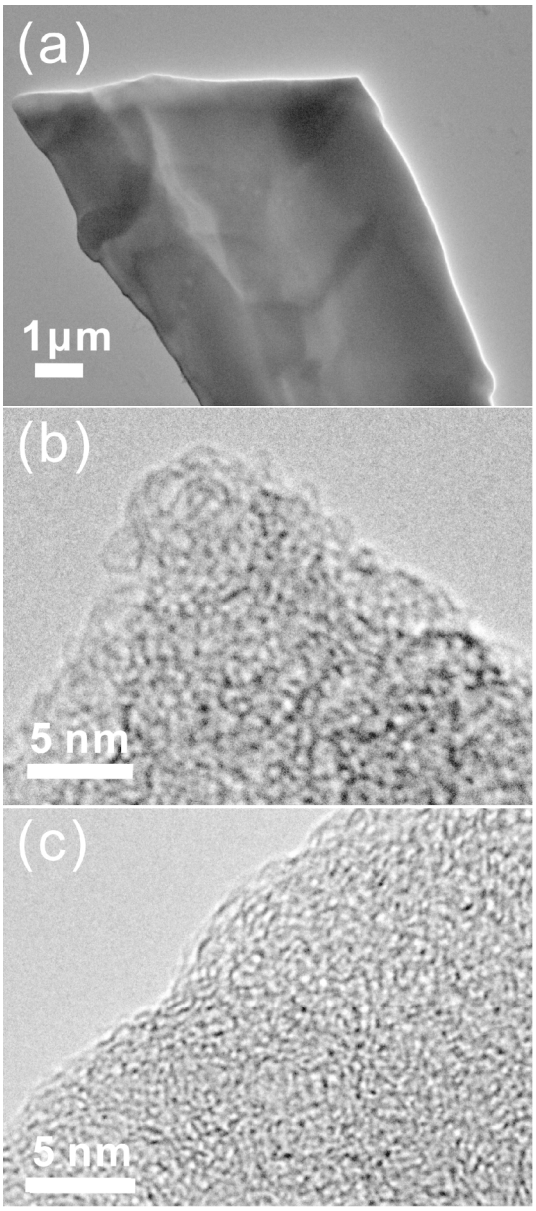

135x307mm (300 x 300 DPI)

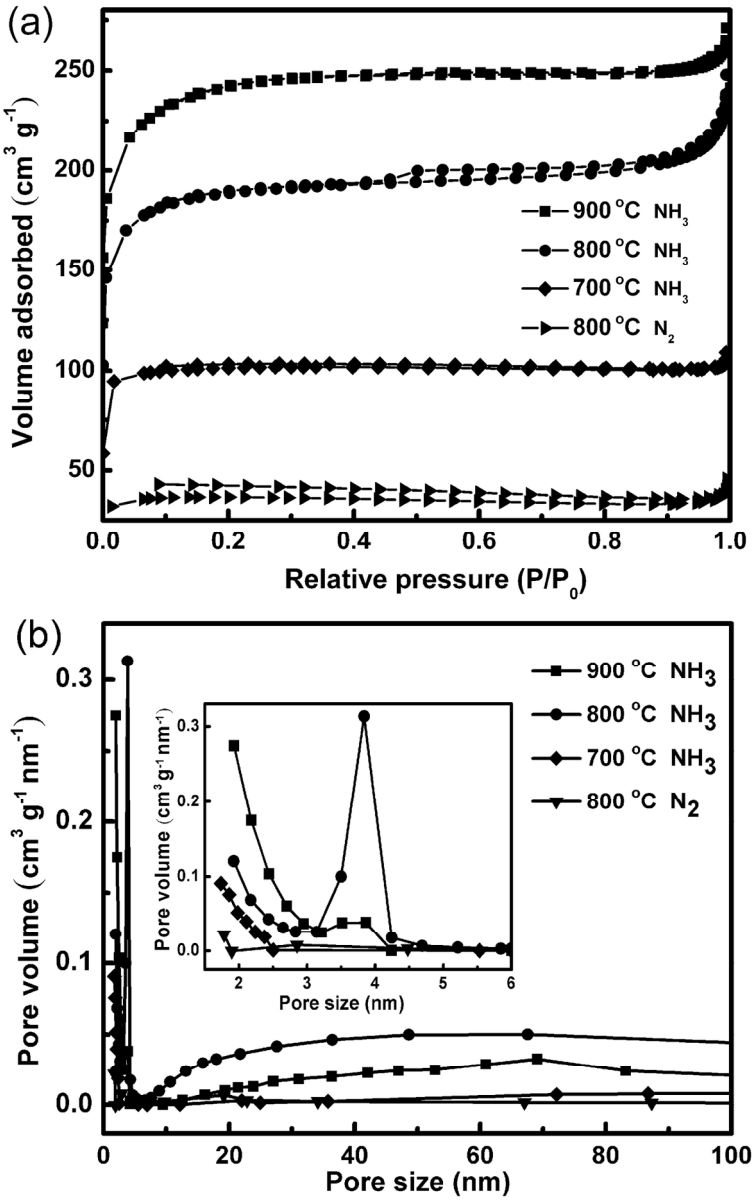

126x199mm (300 x 300 DPI)

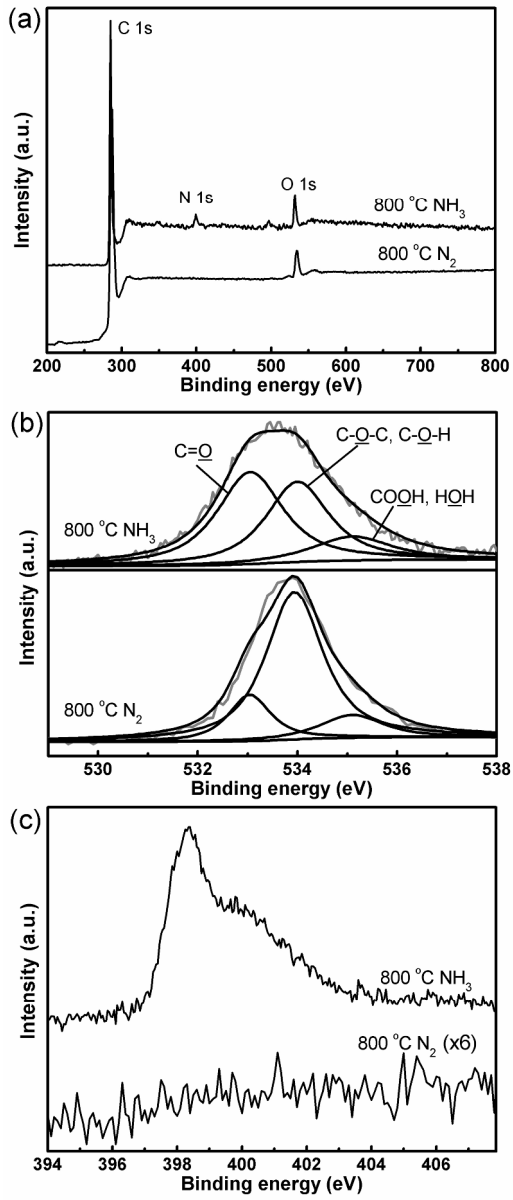

186x433mm (300 x 300 DPI)

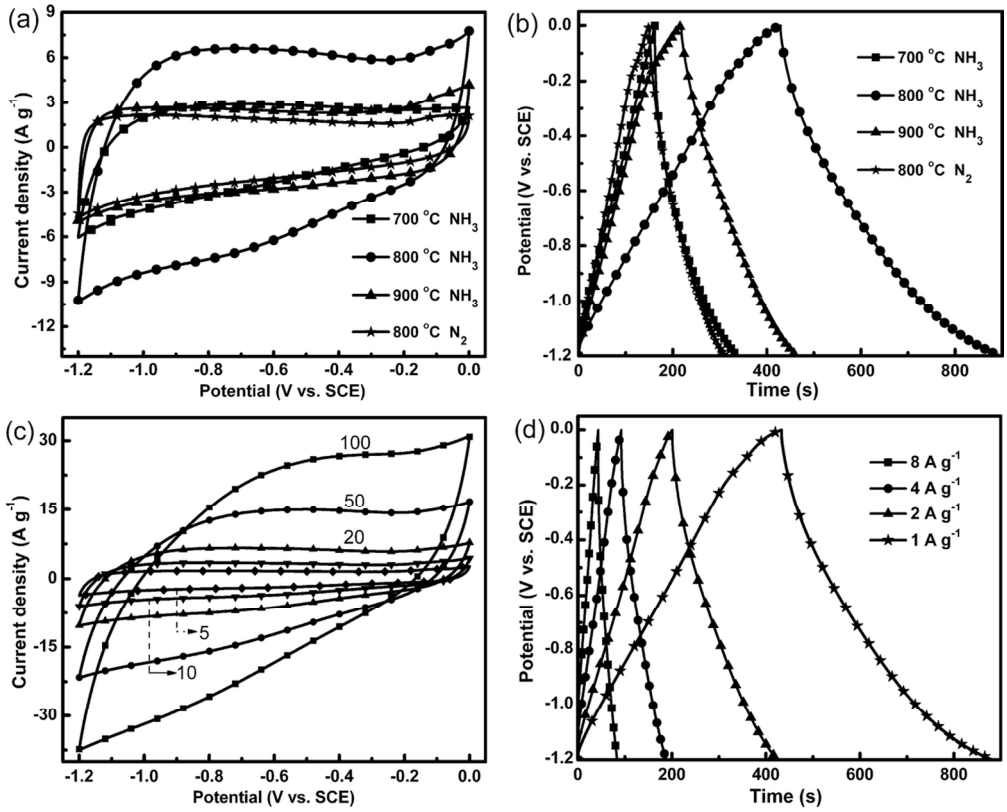

113x91mm (300 x 300 DPI)

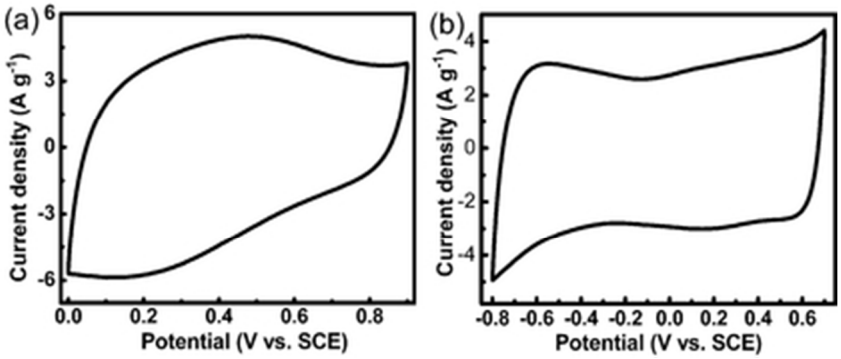

35x15mm (300 x 300 DPI)

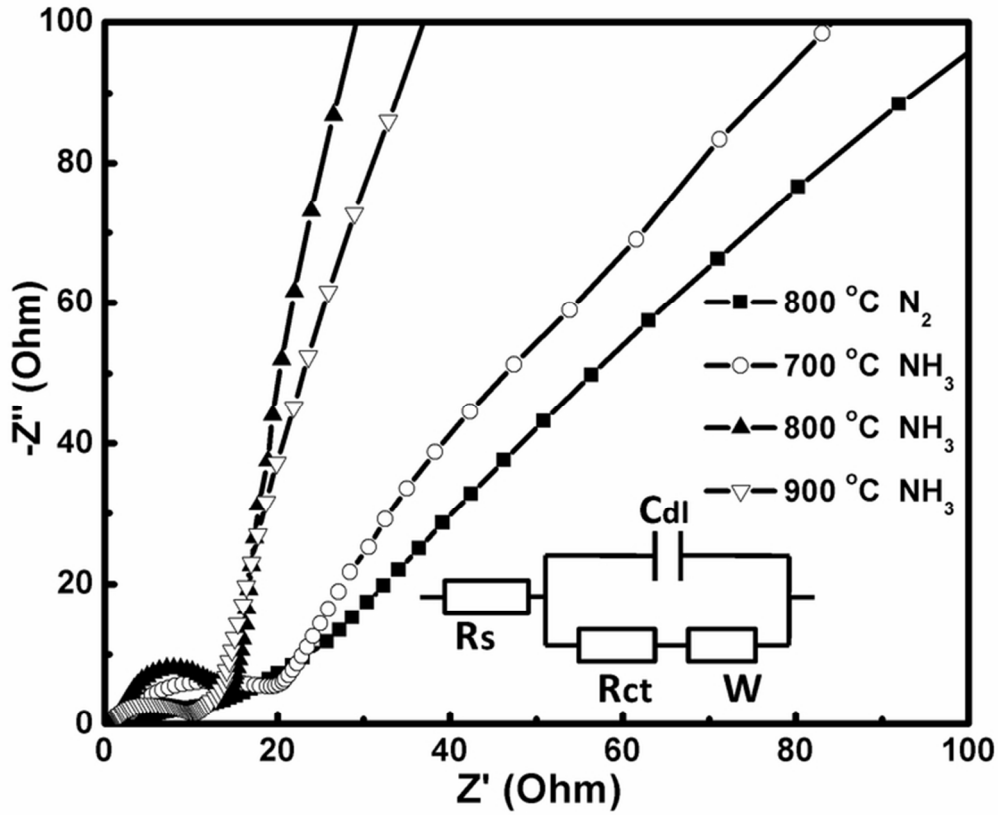

65x53mm (300 x 300 DPI)

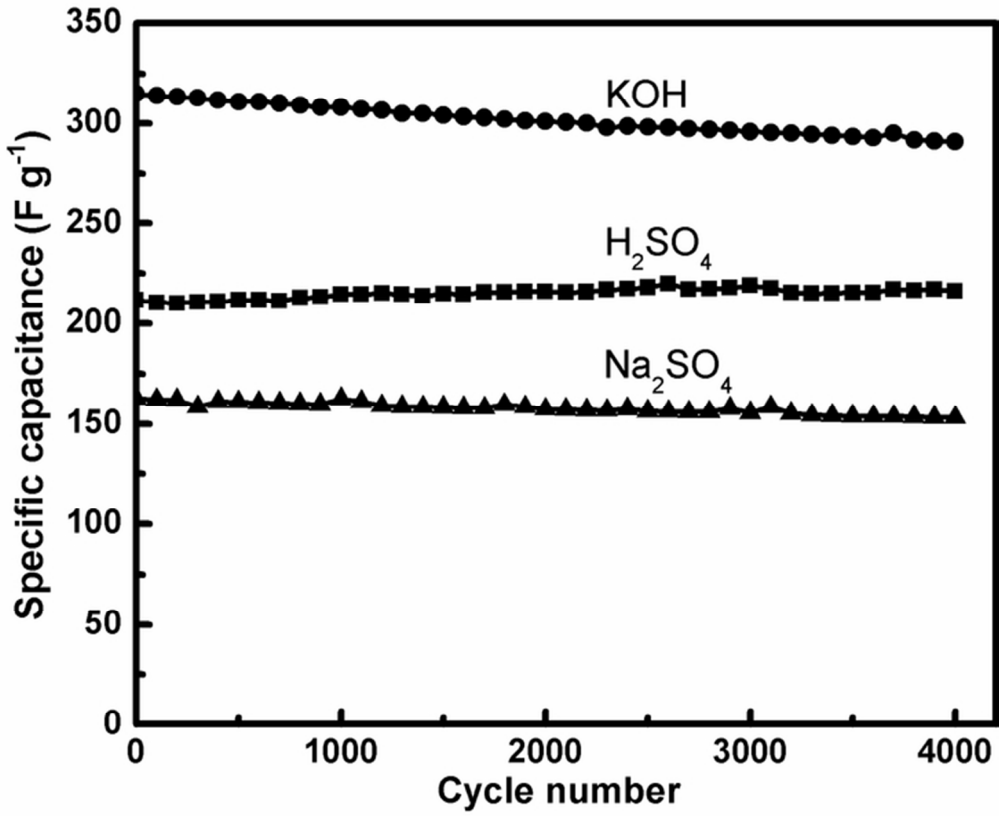

61x50mm (300 x 300 DPI)